Materials Science & Engineering A 793 (2020) 139892

Contents lists available at ScienceDirect

Materials Science & Engineering A

journal homepage: http://www.elsevier.com/locate/msea

A novel ceramic derived processing route for Multi-Principal Element Alloys

M. Gianelle [a], A. Kundu [b], K.P. Anderson [a,1], A. Roy [b], G. Balasubramanian [b], Helen M. Chan [a,*]

[a] Dept. Materials Science & Engineering, Lehigh University, USA
[b] Dept. Mechanical Engineering and Mechanics, Lehigh University, USA

ARTICLE INFO

Keywords:
HEA
Processing
Oxide
Reduction
Microstructure

ABSTRACT

In recent years, Multi-Principal Element Alloys (MPEAs) have emerged as a new and exciting class of materials. To date, the most widely used processing methods for MPEAs are arc melting and mechanical alloying. The study explores the feasibility of an alternative, novel process to process bulk MPEA samples, namely the reduction of an oxide powder precursor mix. Equiatomic CuCoFeNi was selected as a model system of study because these elements form a subset of a large proportion of MPEA compositions already studied. High purity precursor oxide powders of Co_3O_4, CuO, Fe_2O_3 and NiO were milled and mixed using standard ceramic processing methods. The green pellets were subjected to a reduction annealing treatment in flowing 5%H_2–N_2 at 1000 °C, with heat-treatment times ranging from 4 to 1000 h. After 4 h, the sample was transformed into a dense metallic bulk sample with no residual oxides. The microstructure was characterized by x-ray EDS, SEM and XRD, and was shown to consist of a polycrystalline matrix, and a copper-rich second phase situated at the triple points. The hardness was studied by nano-indentation. Using EPMA (electron microprobe analysis), the composition of the matrix was determined to be $Cu_{18.1}Co_{26.6}Fe_{26.9}Ni_{28.4}$ (at%), which represents the single phase MPEA composition. Oxide reduction is a viable technique for processing bulk complex metallic alloys, with potential for novel microstructural tailoring.

1. Introduction

Multi-Principal Element Alloys (MPEAs) are a new class of materials which unlike conventional alloys, comprise multiple (>5) principal components in equimolar or near equimolar ratios [1–6]. The identification of new phases in these systems has been attributed to the increased configurational entropy, hence their original designation as high entropy alloys (HEAs). This concept has opened an expansive realm of unexplored alloy compositions and microstructures, and has attracted significant research interest. The excitement in the field has been fueled by the discovery that for select compositions, the MPEAs exhibit properties that are superior to conventional alloys [7–10]. For example, unlike Inconel 718 or Haynes 230, the MPEA alloys MoNbTaVW and MoNbTaW retain high levels of yield strength up to 1600 °C [9], and hence have potential applications in energy generation and marine turbines. In the realm of low-density alloys, the MPEA $Al_{20}Be_{20}Fe_{10}Si_{15}Ti_{35}$ offers a factor of three improvement in the strength to density ratio compared to most commonly used titanium alloys in the aerospace, marine, and biomedical sectors (Ti–6Al–4V) [7]. In surveying the MPEA literature [2,6], it can be seen that the vast majority of the alloys studied have been fabricated either by melt processes (such as arc melting and induction melting), or mechanical alloying. The goal of the present work was to explore whether MPEAs could be synthesized by a novel method, namely the reduction of an oxide powder mixture. This route for achieving MPEA bodies has several potential advantages. Firstly, it is a solid-state process, so that solute partitioning during cooling from the melt is circumvented. Note that this is a common issue with regard to arc melted structures where there is interdendritic segregation, see for example refs [11–13]. Secondly, by using complex oxides containing multiple cationic species, e.g. spinels or perovskites, one can achieve atomic scale mixing of the metal atoms in the initial powder mix. For example, for an MPEA composition containing both Cu and Fe, it might be advantageous to use delafossite ($CuFeO_2$) as one of the starting oxides, versus CuO and Fe_2O_3. Similarly, a spinel such as $CoFe_2O_4$ could be utilized as a source of both Co and Fe. Further, recent work by the present authors has shown that the partial reduction of mixed oxides can

* Corresponding author.
E-mail address: hmc0@lehigh.edu (H.M. Chan).
[1] Current address: U.S. Naval Research Laboratory, Washington DC, USA.

https://doi.org/10.1016/j.msea.2020.139892
Received 13 May 2020; Received in revised form 29 June 2020; Accepted 2 July 2020
Available online 12 July 2020

lead to metal-ceramic composites with unique hierarchical structures [14–16], hence this may provide an additional mechanism for microstructural tailoring.

For many elemental metals (e.g. Fe, Sn, Cr), the oxide reduction route is a long established process by which they are extracted from their ores. However, this is rarely used as a synthesis technique for metallic alloys. An exception is the work of Verdooren and co-workers, which describes the fabrication of Fe_2O_3 ceramic foam precursors, that were subsequently reduced to closed metallic foam bodies [17,18]. To the authors' knowledge, the only reported application of this technique in the MPEA field is the study by Kenel et al. [19], which addressed a possible method for additive manufacturing of MPEAs. Their work showed that 3D extrusion of inks containing a blend of oxide nanopowders, followed by co-reduction in a pure hydrogen atmosphere, resulted in micro-scaffold structures of near-full density CoCrFeNi. The present study differs from the Kenel et al. work in that it utilizes conventional ceramic powders and processing methods, and the precursor is a pressed ceramic compact.

The equiatomic alloy CoCuFeNi was selected as the proof of concept composition for this study. This subset of metallic elements forms the basis of a large number of transition metal MPEA families, hence any findings would be widely relevant to the MPEA community. Moreover, for the constituent elements, the oxide to metal reductions can be achieved by using forming gas ($5\%H_2$–N_2), which is experimentally more convenient. The CoCuFeNi alloy composition has been the subject of a number of prior studies [20–22]. Liu et al. [20] studied the mechanical behavior of a series of $CoCuFeNiSn_x$ alloys, where the molar ratio of Sn content was varied between zero and 0.1. For tensile testing of the alloy composition CoCuFeNi (i.e., $x = 0$), they reported an ultimate tensile strength of ~470 MPa, and a strain to failure of ~14%. More generally, the study showed that the alloy strength increased with increasing Sn content up to 0.07, and then decreased. In a separate paper, Zheng and co-workers [21] reported that CoCuFeNi exhibited enhanced corrosion resistance relative to 304 stainless steel (NaCl solution, 3.5%). Based on x-ray diffraction (XRD), the microstructure of the alloy was stated to consist of a single phase FCC solid solution.

2. Experimental methods

2.1. Powder processing

The high purity precursor oxide powders utilized were as follows: Co_3O_4 (99.7%), CuO (99.998%), Fe_2O_3 (99.998%), and NiO (99.998%). These were combined in the appropriate proportion so as to yield, on reduction, an equiatomic mixture of Co, Cu, Fe and Ni. The weighed powders were ball milled for 8 h in 200 proof ethanol using alumina milling media. After drying, the powders were compacted into cylindrical pellets (~25 × 5 mm) by uniaxial pressing (5000 psi). For the reduction process, the samples were placed in a graphite crucible and covered with graphite powder. The assembly was subjected to isothermal annealing in a tube furnace with flowing 5% H_2–N_2 (90 cm^3/min). The majority of the heat-treatments were carried out at 1000 °C, with annealing times ranging from 4 to 96 h. The furnace heating and cooling rate was 10 °C/min. For the purposes of comparison, an alloy with the composition CoCuFeNi was also prepared by arc melting. In this case, elemental metal powders (purity $\geq$ 99.9 %, $<$ 60 μm mean particle size) were mixed using a laboratory jar mill (Thomas Scientific Series 8000) at an optimal rotational speed to ensure that the gravitational and centrifugal forces were balanced. The powder mixture was then uniaxially pressed in a steel die at 5000 psi to form disk shaped samples (diameter ~ 20 mm, thickness ~ 3 mm). The pellets were subsequently arc melted on a water-cooled copper hearth enclosed within an argon atmosphere at a pressure of 30 psi (Bühler MAM1). The alloy pellets were inverted and re-melted 4 times to ensure homogeneity of the cast material.

2.2. Characterization

Polished sections of the samples were prepared using standard metallographic techniques. The microstructure of the samples was characterized using scanning electron microscopy (SEM, (Hitachi S-4300 FESEM). Phase identification was carried out using XRD (Malvern Panalytical Empyrean, Bragg-Brentano geometry, Cu-Kα source, 1.54184 Å, 40 kV, 45 mA). Each data set was calibrated with a NIST silicon standard where the XRD patterns of the silicon and the sample were collected at the same time. The XRD patterns were acquired at high resolution, with a 2θ step size of ~0.01°. These results were complemented by electron microprobe analysis (JEOL JXA-8900) and elemental mapping in the SEM. The mechanical behavior of the microconstituents of the processed MPEA was probed using nanoindentation (Hysitron PI-85 Picoindenter) in the SEM (FEI Dual-Beam Scios Focused Ion Beam/Scanning Electron Microscope).

3. Results and discussion

3.1. Microstructure and phase analysis

As mentioned previously, for the purposes of comparison, a metallic alloy with the equiatomic composition CoCuFeNi was prepared by conventional arc melting. As expected, the arc melted alloy exhibited a dendritic structure. Compositional mapping (x-ray EDS) of the as cast structure revealed an inter-dendritic phase that was enriched in copper (see Fig. 1).

Turning now to the samples that were processed via the precursor ceramic route, Fig. 2 shows the XRD data for samples that underwent reduction annealing treatment at 1000 °C for 4, 15, 24 and 100 h. It is important to note that even in the case of the shortest annealing time studied (4 h), there were no detectable peaks that matched either the starting oxides, or any intermediate ceramic compounds. Instead, the spectra corresponded to three metallic phases: one BCC, and two FCC. The diffraction peaks indexed according to the BCC phase closely matched that of FeCo. It follows, therefore, that reduction was essentially complete after 4 h. Given the relative insensitivity of XRD to low volume fractions of second phase (<5 vol%), this result was also confirmed by SEM examination. The FeCo phase was only observed for the 4 h sample, and its existence is believed to derive from transient compositional inhomogeneities due to incomplete powder mixing. The inhomogeneous nature of the initial microstructure, together with the rapid transformation kinetics, rendered any meaningful identification of the sequence of reactions leading to alloy formation difficult. Based on thermodynamic considerations, however, of the four starting oxides the CuO would be expected to reduce the most readily. Some degree of solid state reaction between the oxides is also possible, but this was not detected experimentally. In contrast to the 4 h sample, analysis of the spectra revealed that for the 15–100 h reduction heat-treatments, the sample consisted primarily of two metallic FCC phases with similar lattice parameters. These are designated FCC1 and FCC2.

Polished sections of all of the samples were examined in the SEM. The microstructure of the 4 h sample was highly inhomogeneous. In contrast, the microstructures of samples annealed at 1000 °C for periods ranging from 8 to 100 h were very similar, differing only in the scale of the phases present. A representative microstructure for the 24 h sample is shown in Fig. 3, which depicts x-ray EDS (energy dispersive spectroscopy) elemental maps for each of the constituent metals (Cu, Co, Fe and Ni). To enhance resolution, the elemental maps were collected at a low accelerating voltage (7 kV), and the step size was 100 nm (hence each pixel corresponds to an area of 100 × 100 nm^2). Note that this is at the spatial resolution limit of the SEM-EDS technique itself. The grain size of the matrix was estimated to be ~20 μm. Oxygen mapping did not reveal any residual oxide phases; a result which was consistent with the XRD data. It can be seen that the microstructure consisted of two phases: a copper-rich second phase (A) which was located primarily at triple

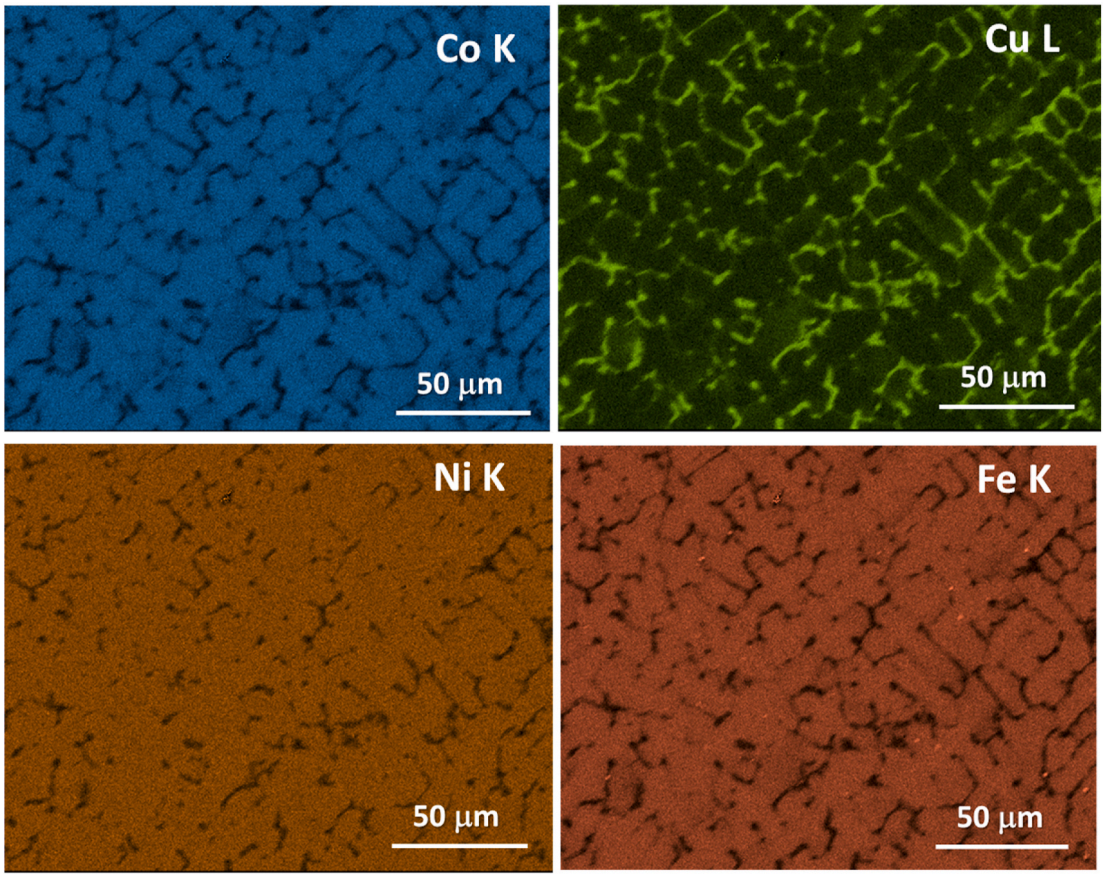

Fig. 1. Arc melted alloy CoCuFeNi. Compositional maps (X-ray EDS) of as cast sample. The maps were collected using an accelerating voltage of 15 kV.

points, and a polycrystalline matrix phase (B). These two microstructural constituents therefore correspond to the two FCC phases identified in the XRD measurements. By comparing the volume fraction of each phase with the XRD peak intensities, it was ascertained that the Cu-rich phase (A) corresponded to FCC1 in the XRD results, and the matrix phase (B) was FCC2. Fig. 3 also reveals that the grain boundary regions were depleted in copper, where the width of these regions is clearly many times greater than the pixel width (100 nm). The reason for this will be discussed in section 3.3.

As can be surmised from Fig. 2(b), the peak positions and hence the lattice parameter of the two FCC phases varied slightly depending on the annealing time. For annealing times <24 h the lattice parameter for the intergranular phase (A) was determined to be 3.617 Å, at 100 h the lattice parameter was 3.612 Å. The lattice parameter of the matrix phase (B) was 3.591 Å for samples annealed times < 24 h, and increased to 3.595 Å for the sample annealed for 100 h. Note that in presenting the lattice parameter data with 4 significant digits, we are taking a conservative approach, estimating the accuracy of peak position as no better than 0.01°, which is equivalent to ~0.001 Å at the (111) peak position.

For the 24 h sample, quantitative compositional analysis of the two phases was carried out using wavelength dispersive spectroscopy (WDS) in the electron microprobe, operated at an accelerating voltage of 15 kV. The compositional data was derived from elemental standards, and the results were corrected for x-ray absorption effects. The results shown in Table 1 represent the average values from 12 (A) and 22 (B) analyzed areas. The expressed uncertainty in the values corresponds to the standard deviation. Note that because each elemental concentration is determined separately using a standard, the total concentration of all the elements may deviate slightly from 100%.

It can be seen that phase A consists of ~80 wt% Cu, with alloying additions of Co (12.2 wt%), Fe (5.0 wt%) and Ni (5.1 wt%). The matrix (B), however, consists of significant weight fractions of each of the alloying elements, and as such is consistent with the compositional definition of an MPEA. Expressed in terms of *atomic %*, the matrix composition is $Cu_{18.1}Co_{26.6}Fe_{26.9}Ni_{28.4}$. This result contrasts with the work of Liu et al. [20] and Zheng et al. [21], which reported the equiatomic composition as single phase.

3.2. Mechanical behavior

Nanohardness testing, utilizing a Berkovich tip, was carried out on a polished section of the CoCuFeNi sample (100 h at 1000 °C). The procedure was automated so as to generate regular arrays of indentation sites. For a given array, the start and end points of the array were labeled with fiduciary marks on the specimen surface. The spacing of the indentation sites was set at ~3 μm. This value was selected based on the CoCuFeNi microstructure (see Fig, 3), and was judged to reasonably ensure sampling of both the intergranular and matrix phases. Note that the selected indent spacing was also sufficiently large to avoid overlap of the strain field between adjacent indents. The total number of indentations across the different indentation arrays was 205. The applied load was 3 mN, resulting in an indentation depth of ~350 nm. For each indentation, values for the reduced modulus and hardness were calculated from the load – displacement data using the Pharr and Oliver method [23]. The results are presented in Fig. 4 in a histogram. It was found that ~74% of the data points was uniformly distributed between 1.875 GPa and 2.625 GPa with a mean hardness value of 2.25 GPa.

Although indentation was carried out in the SEM, the presence of the indenter fixture inhibits the quality of imaging that can be carried out in-situ. For this reason, the indent array was imaged post-indentation. Knowing the indentation sequence, it was possible to use the SEM image of the indentation array to assign a microstructure to any given

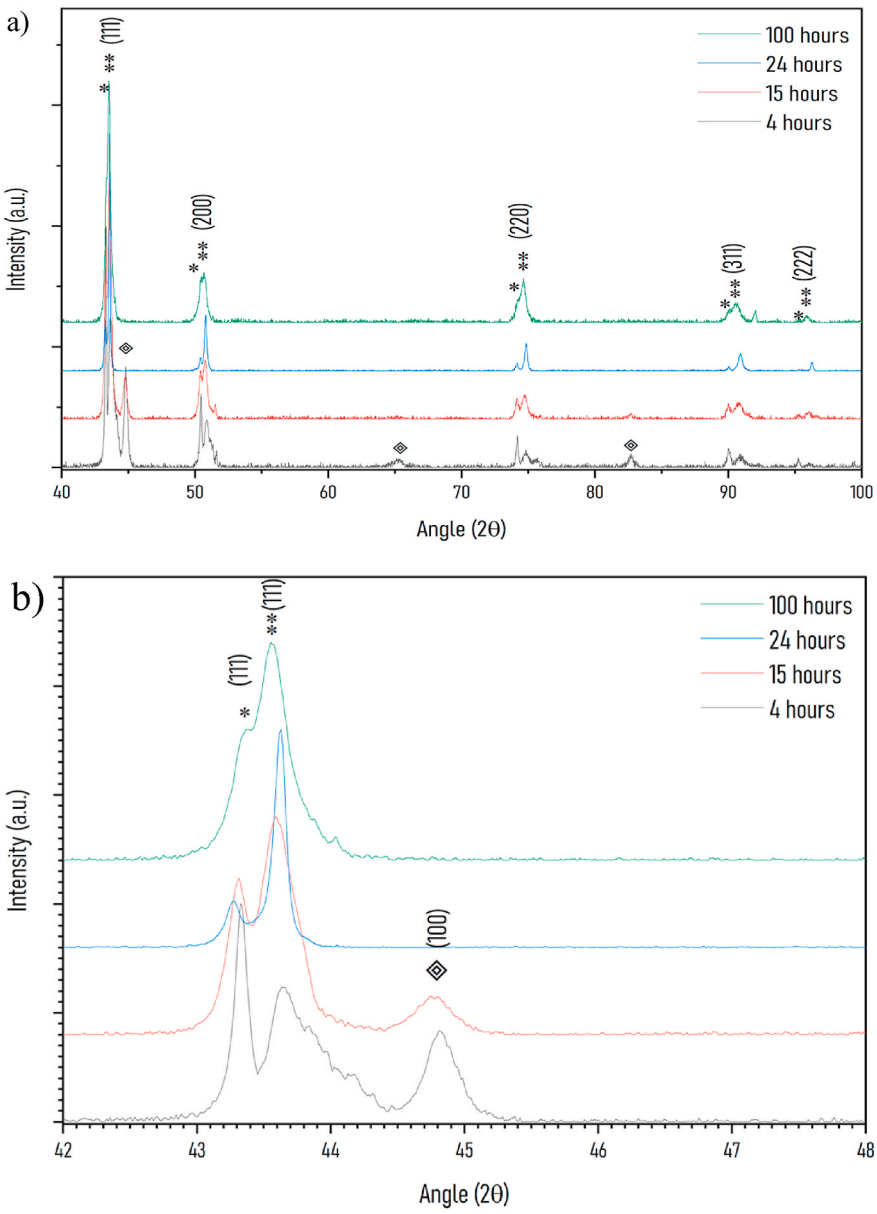

Fig. 2. X-ray diffraction spectra of bulk samples annealed for varying times at 1000 °C in 5% H_2–N_2. a) Wide angle scan (40–100 deg.), b) High resolution scan (42–46 deg.), 2θ step size 0.01 deg. The three distinct phases are designated FCC1 (*), FCC2 (**) and BCC (◈).

data point on Fig. 4. In this manner it was determined that the higher hardness values (>1.875 GPa) corresponded to measurements of the matrix phase. Conversely, the hardness of the copper rich phase was <1.5 GPa. Given that the dimensions of the copper-rich phase were only of the order of a few microns, the proportion of indents that sampled the center of these regions was relatively small (~3%). The hardness values corresponding to those indents were in the range 0.75–1 GPa.

3.3. General

Although previous work [20,21] has described the structure of CoCuFeNi as single phase FCC, our results show that the single phase MPEA in this system has the composition $Cu_{18.1}Co_{26.6}Fe_{26.9}Ni_{28.4}$ (expressed in atomic %). As described previously, from nano-indentation, the hardness of this alloy was determined to be 2.25 ± 0.375 GPa. Using the widely accepted empirical relationship between hardness (H) and strength (σ_{UTS}), where $\sigma_{UTS} \sim H/3$ [24], we can estimate the ultimate tensile strength (σ_{UTS}) of the matrix phase to be ~750 MPa. This compares to a value of ~475 MPa obtained by tensile testing of the CuCoFeNi arc-melt derived sample measured by Liu et al. [20]. Whether the discrepancy is due to the different processing or testing methods is not known at this time.

One noteworthy aspect of the microprobe data was that the magnitude of the uncertainty in the elemental concentrations was much greater than would be expected from statistical x-ray counting considerations alone. One possible explanation is that the variation is due to beam interaction effects. For example, in pure Cu, the beam interaction depth at 15 keV is estimated to be ~0.4 μm [25], therefore although the beam is positioned on the second phase, there may be a contribution in the x-ray signal from sub-surface matrix regions. Another possibility is that the variation in the composition of the second phase is not due to some artefact of the procedure, but rather reflects a true variation in phase composition. Although the phase relationships in the quaternary system Co–Cu–Fe–Ni have not been explored in detail, the ternary phase diagrams corresponding to subsets of these 4 elements have been studied both experimentally and by calculation [26–31]. It has been shown that

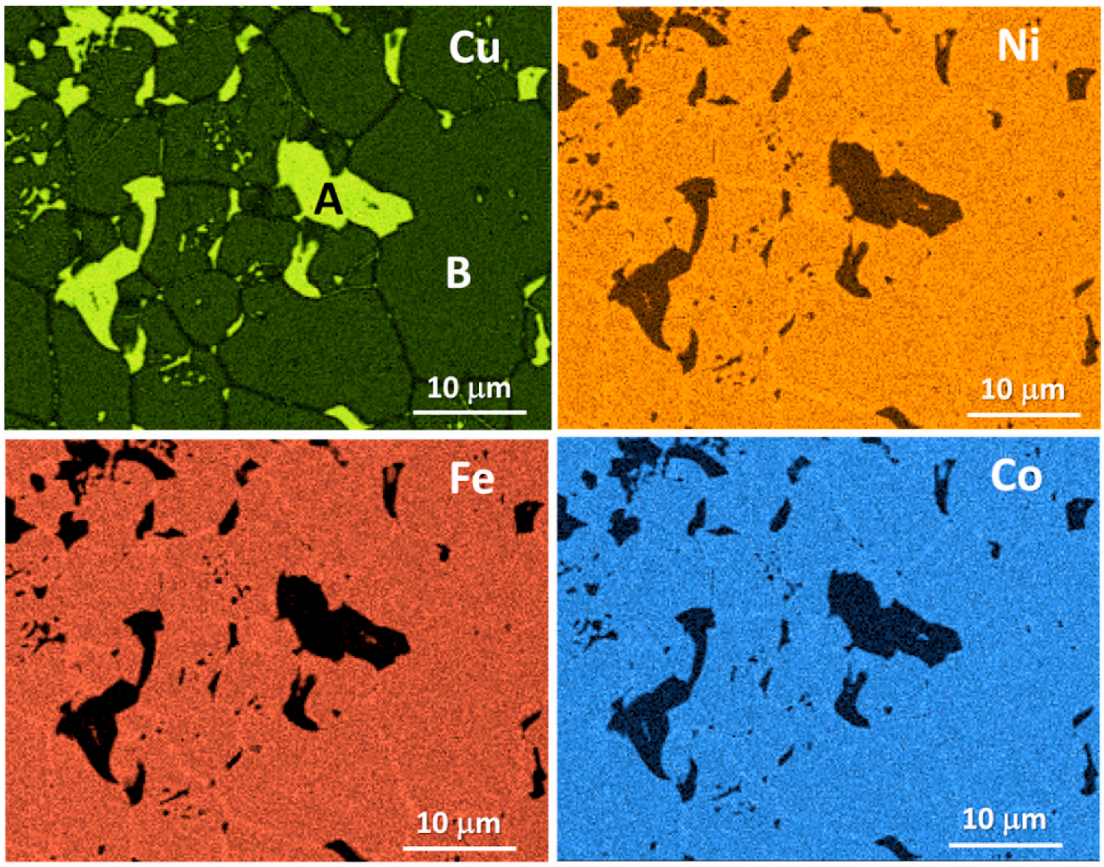

Fig. 3. Compositional maps (X-ray EDS) of sample that had undergone 24 h reduction heat-treatment (1000 °C, 5%H_2–N_2). (7 kV accelerating voltage).

Table 1
Compositional data for sample subjected to 24 h at 1000 °C reduction treatment. Results correspond to microstructural regions depicted in Fig. 2 (A: Intergranular phase, Cu rich, B: matrix phase).

Region	Cu (wt%)	Co (wt%)	Fe (wt%)	Ni (wt%)
A (Second phase)	80.6 ± 6.4	12.2 ± 3.6	5.0 ± 1.3	5.1 ± 1.0
B (Matrix)	19.6 ± 1.1	26.7 ± 2.1	25.5 ± 1.3	28.4 ± 1.3

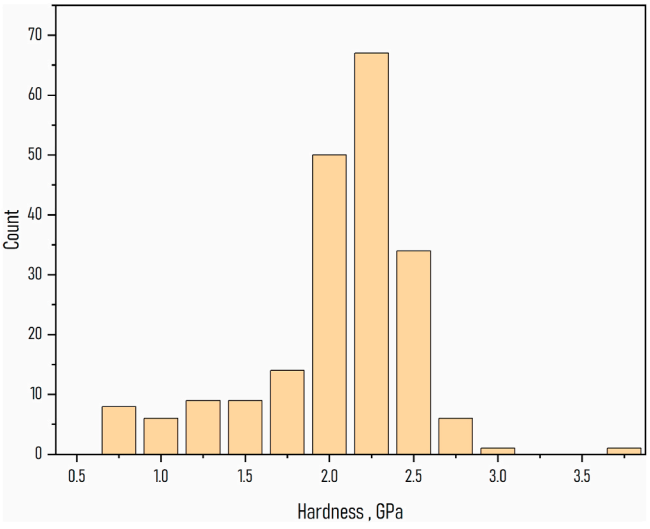

Fig. 4. Nanohardness data of CoCuFeNi sample (24 h at 1000 °C).

for the Cu–Co–Fe [26,27], Cu–Ni–Fe [28], and Cu–Co–Ni [29,30] systems, a miscibility gap occurs between two FCC phases, one of which is copper rich. At any given temperature, the exact composition of the two phases in equilibrium is dictated by the overall composition and the intersecting set of tie lines. It is also well established that with decreasing temperature, the extent of the miscibility gap increases, and the copper content of the copper-rich component increases. It seems plausible, therefore, that the composition of the second phase will depend locally on the cooling rate, and the extent to which it can equilibrate with the surrounding matrix. In this regard, it is suggested that during cooling, there is net diffusion of copper atoms from the matrix to the copper rich phase. The enhanced GB diffusion kinetics result in the observed depletion of copper at the boundaries (see Fig. 3).

The current study has focused on the use of 5% H_2–N_2 as the reduction atmosphere. As mentioned in the introduction, this is experimentally convenient as it is below the explosive limit for hydrogen. Clearly, the partial pressure of oxygen (pO_2) is an important processing parameter for this technique. Depending on the stability of the associated oxide, more highly reducing gas atmospheres (e.g. 100% H_2) may be required. In the case of extremely stable oxides (e.g. Al_2O_3, ZrO_2, TiO_2), achieving the required pO_2 level for bulk reduction is possible in principle, but experimentally very challenging, and hence economically impractical for a commercial process. In such cases, exploring non-oxide precursors is a possible alternative. For example, Seki and Yamaura [32] have reported the reduction of titanium oxide to titanium via the formation of titanium nitride as an intermediate compound.

The study also raises interesting issues as to the influence of processing on MPEA microstructure. Ghazi and Ravi [33] suggested that the difference between MPEAs synthesized by arc melting versus mechanical alloying was that the approach to equilibrium was different, i.e. in the case of arc melting, the change in microstructure corresponds to cooling from elevated temperature (through the liquid state), whereas

for mechanical alloying, the microstructure development is closer to what would be expected from heating from room temperature. The oxide reduction method is more akin to the latter. It follows that although both the arc melted and oxide derived CoCuFeNi exhibit a copper-rich constituent (see Figs. 2 and 3), the *origin* of that phase is different. In the case of the arc melted alloy, the interdendritic phase is an example of the microsegregation that is commonly observed for melt-derived samples. It occurs as a result of partitioning of the excess solute into the liquid. For the oxide derived sample, however, as per the prior discussion, the copper rich phase forms according to phase relationships in the solid state. For the CoCuFeNi composition that was the subject of the present study, the second phase compositions appear generally similar, but this is not necessarily true for other MPEAs.

In principle, using the oxide reduction technique, intermediate phases/compounds that form only during cooling from the melt can be avoided. Moreover, by judicious choice of starting powders and exploiting differences in oxide reduction rates under different conditions, it may be possible to impose a desired reaction sequence between pairs or groups of metallic elements. This could be used, for example, to increase the volume fraction of a desirable constituent, or perhaps minimize the formation of deleterious intermetallic compounds.

4. Summary

The study demonstrated that the reduction of a compacted oxide mixture (Co_3O_4, CuO, Fe_2O_3 and NiO) is a viable technique for fabricating bulk metallic CoCuFeNi. The microstructure of the resultant alloy was polycrystalline and consisted of two phases, a polycrystalline matrix and an intergranular phase that was Cu-rich. The composition of the matrix (at.%) was $Cu_{18.1}Co_{26.6}Fe_{26.9}Ni_{28.4}$, and the study shows that this, rather than the equiatomic formula, is the more accurate representation of the single phase MPEA composition for these four elements. The study has shown that the reduction of ceramic powders is a viable technique for achieving polycrystalline MPEAs, and has the potential to form microstructures that are different from that of conventional metal forming processes. Further microstructural tailoring could be achieved by exploring different precursor powder compositions and reduction conditions.

Data availability

The raw/processed data required to reproduce these findings cannot be shared at this time due to technical limitations.

Declaration of competing interest

The authors declare that they have no known competing financial interests or personal relationships that could have appeared to influence the work reported in this paper.

CRediT authorship contribution statement

M. Gianelle: Investigation, Formal analysis. **A. Kundu:** Supervision, Investigation, Conceptualization, Writing - review & editing, Formal analysis. **K.P. Anderson:** Investigation, Formal analysis. **A. Roy:** Investigation. **G. Balasubramanian:** Supervision, Resources. **Helen M. Chan:** Project administration, Supervision, Writing - original draft, Conceptualization.

Acknowledgements

This work was funded by the National Science Foundation under DMR Grant #1507955 and CMMI Grant #1944040. Partial support of M. Gianelle from the Henry Luce Foundation is also gratefully acknowledged.

References

[1] M.H. Tsai, J.W. Yeh, High entropy alloys: a critical review, Mater. Res. Lett. 2 (2014) 107–123.
[2] D.B. Miracle, O.N. Senkov, A critical review of high entropy alloys and related concepts, Acta Mater. 122 (2017) 448–511.
[3] E.J. Pickering, N.G. Jones, High-entropy alloys: a critical assessment of their founding principles and future prospects, Int. Mater. Rev. 61 (2016) 183–202.
[4] M.C. Gao, J.-W. Yeh, P.K. Liaw, Y. Zhang, High-entropy Alloys: Fundamentals and Applications, Springer Publishing Co., New York, NY, 2016.
[5] B.S. Murty, J.W. Yeh, S. Ranganathan, High-entropy Alloys, Butterworth-Heinemann, June 21, 2014.
[6] O.N. Senkov, D.B. Miracle, K.J. Chaput, J.P. Couzinie, "Development and exploration of refractory high entropy alloys—a review, J. Mater. Res. 33 (2018) 3092–3128.
[7] A. Gali, E.P. George, Tensile properties of high and medium entropy alloys, Intermetallics 39 (2013) 74–78.
[8] C.Y. Hsu, C.C. Juan, W.R. Wang, T.S. Sheu, J.W. Yeh, S.K. Chen, On the superior hot hardness and softening resistance of $AlCoCr_xFeMo_{0.5}Ni$ high-entropy alloys, Mater. Sci. Eng. A 528 (2011) 3581–3588.
[9] O.N. Senkov, G.B. Wilks, J.M. Scott, D.B. Miracle, Mechanical properties of $Nb_{25}Mo_{25}Ta_{25}W_{25}$ and $V_{20}Nb_{20}Mo_{20}Ta_{20}W_{20}$ refractory high entropy alloys, Intermetallics 19 (2011) 698–706.
[10] P. Lu, J.E. Saal, G.B. Olson, T. Li, O.J. Swanson, G.S. Frankel, A.Y. Gerard, K. F. Quiambao, J.R. Scully, Computational materials design of a corrosion resistant high entropy alloy for harsh environments, Scripta Mater. 153 (2018) 19–22.
[11] Y.P. Wang, B.S. Li, M.X. Ren, C. Yang, H.Z. Fu, Microstructure and compressive properties of AlCrFeCoNi high entropy alloy, Mater. Sci. Eng. A 491 (2008) 154–158.
[12] X.W. Liu, L. Liu, G. Liu, X.X. Wu, D.H. Lu, J.Q. Yao, W.M. Jiang, Z.T. Fan, W. B. Zhang, The role of carbon in grain refinement of cast CrFeCoNi high-entropy alloys, Met. Mater. Trans. A49 (2018) 2151–2160.
[13] A.M. Manzoni, H.M. Daoud, R. Voelkl, U. Glatzel, N. Wanderka, Influence of W, Mo and Ti trace elements on the phase separation in $Al_8Co_{17}Cr_{17}Cu_8Fe_{17}Ni_{33}$ based high entropy alloy, Ultramicroscopy 159 (2015) 265–271.
[14] Z. Yu, M. Kracum, A. Kundu, M.P. Harmer, H.M. Chan, Microstructural evolution of a Cu and θ-Al_2O_3 composite formed by reduction of delafossite $CuAlO_2$: a HAADF-STEM study, Cryst. Growth Des. 16 (2016) 380–385.
[15] K. Anderson, R.P. Vinci, H.M. Chan, Novel metal-ceramic composite microstructures produced through the partial reduction of $CoTiO_3$, J. Mater. Sci. 53 (2018) 8193–8210.
[16] M. Kracum, C.J. Marvel, M. Albu, F. Hofer, M.P. Harmer, H.M. Chan, Copper-alumina nano-composites derived from $CuAlO_2$: phase transformation and microstructural coarsening, J. Am. Ceram. Soc. 101 (2018) 5801–5810.
[17] A. Verdooren, H.M. Chan, J.L. Grenestedt, M.P. Harmer, H.S. Caram, Production of metallic foams from ceramic foam precursors, Adv. Eng. Mater. 6 (2004) 397–399.
[18] A. Verdooren, H.M. Chan, J.L. Grenestedt, M.P. Harmer, H.S. Caram, Fabrication of ferrous metallic foams by reduction of ceramic foam precursors, J. Mater. Sci. 40 (2005) 4333–4339.
[19] C. Kenel, N.P.M. Casati, D.C. Dunand, 3D ink-extrusion additive manufacturing of CoCrFeNi high-entropy alloy micro-lattices, Nat. Commun. 10 (2019), 904.
[20] L. Liu, J.B. Zhu, C. Zhang, J.C. Li, Q. Jiang, Microstructure and the properties of $FeCoCuNiSn_x$ high entropy alloys, Mater. Sci. Eng. 548 (2012) 64–68.
[21] Z.Y. Zheng, X.C. Li, C. Zhang, J.C. Li, Microstructure and corrosion behaviour of $FeCoNiCuSn_x$ high entropy alloys, Mater. Sci. Technol. 31 (2015) 1148–1152.
[22] S. Praveen, B.S. Murty, R.S. Kottada, Phase evolution and densification behavior of nanocrystalline multicomponent high entropy alloys during spark plasma sintering, J. Oper. Manag. 65 (2013) 1797–1804.
[23] G.M. Pharr, W.C. Oliver, Measurement of thin film mechanical properties using nanoindentation, MRS Bull. 17 (1992) 28–33.
[24] P. Zhang, S.X. Li, Z.F. Zhang, General relationship between strength and hardness, Mater. Sci. Eng. A 529 (2011) 62–73.
[25] K. Kanaya, S. Okayama, Penetration and electron loss theory of electrons in solid targets, J. Phys. D Appl. Phys. 5 (1972) 43–58.
[26] M. Palumbo, S. Curiotto, L. Battezzati, "Thermodynamic analysis of the stable and metastable Co–Cu and Co–Cu–Fe phase diagrams, Calphad 30 (2006) 171–178.
[27] S. Bein, C. Colinet, M. Durand-Charre, "CVM calculation of the ternary system Co–Cu–Fe,", J. Alloys Compd. 313 (2000) 133–143.
[28] K.J. Ronka, A.A. Kodentsov, P.J.J. Van Loon, J.K. Kivilahti, F.J.J. Van Loo, Thermodynamic and kinetic study of diffusion paths in the system Cu-Fe-Ni, Metall. Mater. Trans. 27A (1996) 2229–2238.
[29] M. Hasebe, K. Oikawa, T. Nishizawa, Computer calculation of phase diagrams for Co-Cu-Mn and Co-Cu-Ni systems, J. Jap. Inst. Met. 46 (1982) 584–690.
[30] S. Curiotto, L. Battezzati, E. Johnson, N. Pryds, "Thermodynamics and mechanism of demixing in undercooled Cu–Co–Ni alloys, Acta Mater. 55 (2007) 6642–6650.
[31] P. Villars, A. Prince, H. Okamoto, Handbook of Ternary Alloy Phase Diagrams, vol. 6, ASM, 1995, pp. 8178–8192.
[32] I. Seki, S. Yamaura, Reduction of titanium dioxide to metallic titanium by nitridization and thermal decomposition, Mater. Trans. 58 (2017) 361–366.
[33] S.S. Ghazi, K.R. Ravi, Phase-evolution in high entropy alloys: role of synthesis route, Intermetallics 73 (2016) 40–42.